




A fully-textile wideband AMC-backed antenna for wristband WiMAX and medical applications

cambridge.org/mrf

Mohamed El Atrash¹ , Mahmoud A. Abdalla²  and Hadia M. Elhennawy¹ 

¹Department of Electronics and Communications, Ain Shams University, Abbaseya, Cairo, Egypt and ²Department of Electronic Engineering, Electromagnetic Waves Group, Military Technical College, Cairo, Egypt

Research Paper

Cite this article: El Atrash M, Abdalla MA, Elhennawy HM (2021). A fully-textile wideband AMC-backed antenna for wristband WiMAX and medical applications. *International Journal of Microwave and Wireless Technologies* **13**, 624–633. <https://doi.org/10.1017/S1759078720001397>

Received: 21 June 2020
Revised: 13 September 2020
Accepted: 14 September 2020
First published online: 14 October 2020

Key words:

Artificial magnetic conductor; low SAR; textile; wearable applications; wideband; WiMAX

Author for correspondence:

Mohamed El Atrash,
E-mail: mzaky@msa.eun.eg

Abstract

Proposed is a wideband, low profile, fully flexible, and all-textile-based slotted triangular antenna loaded with a 2×2 textile-inspired artificial magnetic conductor to be worn on the wrist. The integrated antenna design is designed to cover the frequency band from 3.1 to 6.5 GHz. The integrated design has two main resonances, where the first one is at 3.5 GHz, which can serve the WiMAX communication standard, while the second is at 5.8 GHz, which can serve the Industrial, Scientific and Medical (ISM)-band. The incorporated textile materials are composed of the conductive and dielectric fabrics that are realized by ShieldIt and Felt, respectively. When simulated against the human model wrist, the integrated antenna design displayed a realized gain of 6.71 dBi and radiation efficiency of 79.1%, at 3.5 GHz. Furthermore, at 5.8 GHz, it displayed a realized gain of 7.82 dBi and total efficiency performances of 66.1%. Moreover, it accomplished very low SAR levels within the antenna frequency band. Averaged over 1 g of tissue, it exhibited maximum SAR levels of 3.28×10^{-6} and 9.37×10^{-7} W/kg at 3.5 and 5.8 GHz, respectively. For the bent scenarios, the integrated antenna design displayed robustness when bent at an angle of 20 and 40°. Finally, measurement results are illustrated and analyzed. Based on the presented results, the suggested all-textile integrated antenna design might be designated for integration with the wristband to monitor the user health conditions through many possible frequency channels.

Introduction

Wearable devices have tremendously grown over the years due to the limitless on-body and off-body applications demanding such technology [1]. For instance, army, sports, saving lives duties, and smart wearable devices are some of the applications necessitating wearable technology. The wrist is considered the most attractive human part to monitor the human health, as various vital signs can be measured at it, such as the blood pressure and pulse rate. Using the wearable device, wireless transmission of such information to a physician for analysis and evaluation is valid. In that way, physicians can take quick decisions to save human lives.

Wearable devices require antennas of certain characteristics. For instance, being of small size for appealing purposes, flexible to a certain degree to accommodate the user orientation and posture, high in gain and efficiency, exhibiting directional radiation pattern to reduce back radiations absorbed by the human body, and thus, displaying low specific absorption rate (SAR). According to the published literature, monopole and patch antenna types are suitable for wearable antennas, where they have utilized substrate materials as dielectric textiles [2–20], ultra-thin polyimides [21–23], and composite materials [24, 25] to attain flexibility.

In specific applications point of view, the need for health monitoring applications has pushed the research for using multi-band frequency channels using the same antenna [26]. To satisfy this trend, different wearable antennas were presented using different design approaches to attain multi-band and wideband resonances [27–35]. Through the design of these antennas, they were required to have a small effect on the human body by demonstrating low SAR. SAR measures the amount of power radiated and absorbed by the human body. It is worth to mention that the Federal Communications Commission (FCC) and International Electrotechnical Commission (IEC) have set two renowned standards of 1.6 W/kg, averaged over 1 g tissue, and 2 W/kg, averaged over 10 g tissue, respectively, where all wearable antennas should abide to.

For achieving a directional radiation pattern leading to enhancements in gain and reductions in SAR levels, the wearable antenna is backed with a reflector referred to as an artificial magnetic conductor (AMC), often termed electromagnetic band gap (EBG) structures [2–5, 21]. Additionally, metasurfaces [6] and substrate-integrated waveguide cavities [7] were utilized as backing structures for shielding purposes. Furthermore, reported in [8–20] and [24, 25] are simple ground planes incorporated to decouple the antenna from the human body. Nevertheless, ground planes, recognized as perfect electric conductors, suffer from the out-of-phase reflection feature, which leads to a sudden drop in the total efficiency and storage

of energy in the antenna near-field region [36]. Another conventional method is to increase the air-gap separation in-between the wearable antenna and the human body [22, 23]. Despite its success, it leads to an increase in the overall form factor; therefore, the tradeoff of performance against size.

It is challenging to attain a wideband wearable antenna that is high in gain and radiation efficiency, as well as possesses a high degree of flexibility. For instance, in [5] and [37–39], conformable wearable antennas that achieved high gain and radiation efficiency performance parameters were proposed. However, they did not possess a wideband resonance specification.

As such, proposed in this paper is an all-textile slotted triangular monopole antenna that is backed by an all-textile 2×2 AMC array structure, which is referred to throughout the paper as the integrated design. The integrated design is wideband, compact in size, highly conformable, demonstrates high gain, and exhibits low SAR levels when operating at close distances from the human body. Compared to all reported work in literature, the wideband along with the compactness, high gain, and flexibility is one major contribution. Also, the whole integrated textile antenna is another contribution which makes the antenna suitable for many applications. Finally, the paper presents a comparison between textile and other materials. With such form factor and performance, the integrated design can be integrated into wristbands to monitor the user's vital signs; thus, it serves as a good candidate for WiMAX and medical applications. Conducted in section "The flat all-textile integrated design performance against the human wrist" is the flat simulated and tested results, along with analysis, against the specific anthropomorphic mannequin (SAM) human model and user's wrist. Moreover, presented is a study on the pros of realizing an all-textile design over an all-polyimide-based design. Finally, highlighted in section "The bent all-textile integrated design performance against the human wrist" is the bent integrated antenna design performance over the SAM and a subject's wrist.

The flat all-textile integrated design performance against the human wrist

The all-textile integrated design comprises a slotted-triangular co-planar waveguide (CPW) fed antenna loaded with a 2×2 AMC array arrangement. The full methodology of how the design was achieved, including the effects of the incorporated slots, is found in [21]. It is worth noting that a 2×2 array size was specifically selected to maintain the low profile feature of the overall integrated design. The added value in the proposed work than [21] is that the proposed one is all-textile based to integrate with a wristband worn by athletes for monitoring the user's health conditions, such as blood pressure and pulse rate, at the wrist. Such valuable information is then transmitted wirelessly to a physician for diagnosing the vital signs. Moreover, the all-textile proposed work attained wideband resonance, whereas that in [21] was dual-band. Finally, by realizing an all-textile design, the proposed design is highly flexible, which is desired for wearable applications.

Figure 1(a) illustrates the top view of the monopole antenna and Fig. 1(b) displays the top view of the 2×2 AMC array structure. Moreover, depicted in Fig. 1(c) are the fabricated prototypes of each structure, which are highly compact in comparison with a one-pound coin. However, techniques such as designing the antenna based on the composite right/left-handed transmission line methodology [14, 18, 40], as well as the fractal design concept [27], could further reduce the antenna size. The patch and ground

structures are realized using the conductive textile ShieldIt Super [41]. It possesses a thickness of 0.17 mm and an estimated conductivity of 1.18×10^5 S/m. The antenna and AMC substrates are made of Felt [42], with the difference being in the thicknesses. For the monopole antenna, the substrate thickness is 1.5 mm, while that for the AMC is 3 mm. Felt has a relative permittivity and loss tangent of 1.2 and 0.044, respectively. When integrated, both structures are separated by 3 mm, which, practically, is realized by foam.

Since the motivation behind the proposed work is to design an all-textile wearable antenna for human wrist applications, the integrated design performance was assessed at 3 mm from the SAM human hand phantom, as illustrated in Fig. 2. Such a separation was intentionally left for the wristband on which the design will be integrated onto. The SAM can be found in the Computer Simulation Technology (CST) software tool libraries. It consists of a liquid, enclosed by a shell, which emulates a human tissue. It possesses a relative permittivity, conductivity, and mass density of 37.005, 2.0249 S/m, and 1090 kg/m³, respectively. The benefit of utilizing the SAM hand phantom, in the simulations, is that it is time-efficient in determining the SAR levels. At such setup, the all-textile integrated design was evaluated in terms of its performance parameters.

Depicted in Fig. 3 enclosure is the arrangement for measuring the all-textile flat integrated design fabricated prototype reflection coefficient over a subject's wrist. Rohde & Schwarz ZVB20 Vector Network Analyzer (VNA) was incorporated for conducting the measurement. As observed, the integrated design is mounted over a wristband to imitate the scenario targeted. The simulated (solid black) and measured (dotted red) reflection coefficients are benchmarked against one another in Fig. 3. Courtesy of the thick textile-based AMC material, and with respect to the -6 dB threshold, the integrated design displayed a simulated wideband resonance ranging from 3.2 to 6.8 GHz (-6 dB impedance bandwidth of 3.6 GHz), whereas the measured result achieved a wider bandwidth ranging from 2.8 to 7 GHz (with a -6 dB bandwidth of 4.2 GHz).

The slight discrepancies between both sets of results could be attributed to the fact that fabrication was done manually, where the thin slots are not as accurate as the simulated design. Such narrow separations are very subtle and greatly manipulate the results. This is also the case for the fabricated dual-band AMC, where it is clear that the fabricated square patches are not as accurate as the simulated ones. Finally, the simulation environment does not take into consideration the presence of the different subjects and objects that are in the measurement environment.

Thanks to the AMC array arrangement, the integrated antenna design possessed the patch-like unidirectional radiation pattern, which is highly desirable for wearable applications. In other words, the back radiations, which were toward the human body, were minimized and reflected in the opposite direction with respect to the human body. This justifies the high gain values achieved within the wideband spectrum, as observed in Fig. 4. Observing the left Y-axis scale of Fig. 4, the realized gain varied from 5 to 8.3 dBi; however, with a reduction to 3.5 dBi at 4.8 GHz. Moreover, perceiving the right Y-axis scale of Fig. 4, the radiation efficiency varied from 58 to 81%; though, with a reduction to 50% at 4.8 GHz. The reductions exhibited at 4.8 GHz are acceptable for textile wearable antennas and are close and better than the average of [25]. Moreover, the gain at 4.8 GHz is 4 dBi, which differs from the realized gain that takes into consideration the matching losses.

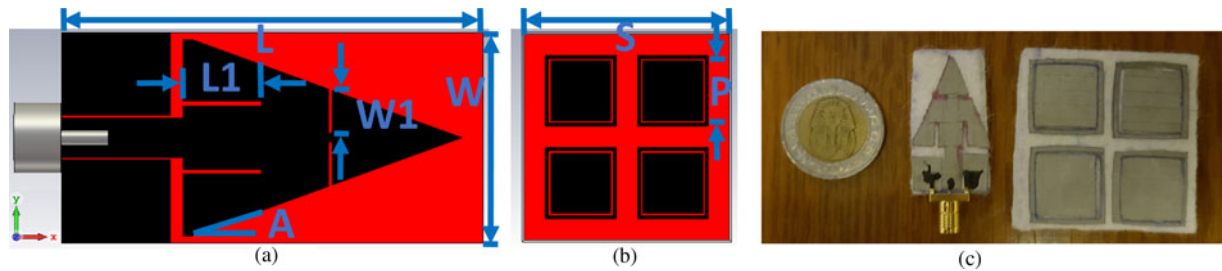


Fig. 1. The textile-integrated design separate structures 2D layout top view: (a) Monopole antenna ($L = 36$ mm, $W = 18$ mm, $L_1 = 6.5$ mm, $W_1 = 3.14$ mm, $A = 20^\circ$); (b) AMC array ($S = 45.3$ mm, $P = 20.3$ mm); (c) Fabricated all-textile prototype, demonstrating compactness against a one pound coin.



Fig. 2. The integrated design flat layout against the SAM human hand model.

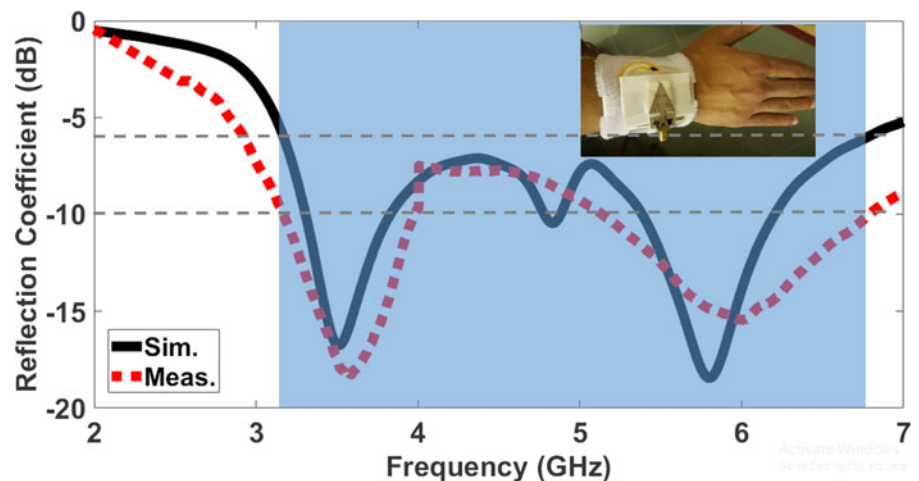


Fig. 3. Comparison between the simulated and measured flat integrated design reflection coefficients against the human wrist, with an inset of the setup for measuring the fabricated prototype reflection coefficient.

Focusing on the two main resonant frequencies of 3.5 and 5.8 GHz of the Industrial, Scientific, and Medical (ISM)-band, the integrated antenna design attained a peak realized gain of 6.71 and 7.82 dBi, respectively. Furthermore, it achieved good radiation efficiencies of 79.1 and 66.1%, respectively. Hence, it can be concluded that the antenna is robust against human hand loading, since it maintained its wide-band resonance, along with high gain and radiation efficiency performances.

For the sake of comparison, and to show the good achieved characteristics of the designed textile antenna, presented in this section, as well, is a study on the advantage of utilizing textile materials over polyimide materials. The antenna substrate

materials included the 1.5 mm-thick Felt and 0.1 mm-thick Rogers ULTRALAM 3850. Moreover, the AMC substrate materials included the 3 mm-thick Felt and 1.52 mm-thick RO3003. Such materials were specifically chosen to match those incorporated in [21].

Displayed in Fig. 5 is the reflection coefficient of the proposed all-textile design benchmarked against that of the polyimide-based design when evaluated nearby the SAM human hand phantom. As perceived, the all-textile design achieved wideband resonance, with respect to the -6 dB threshold, ranging from 3.2 to 6.8 GHz, courtesy of the thick textile-based AMC material. This feature was lost when evaluating the all-polyimide-based

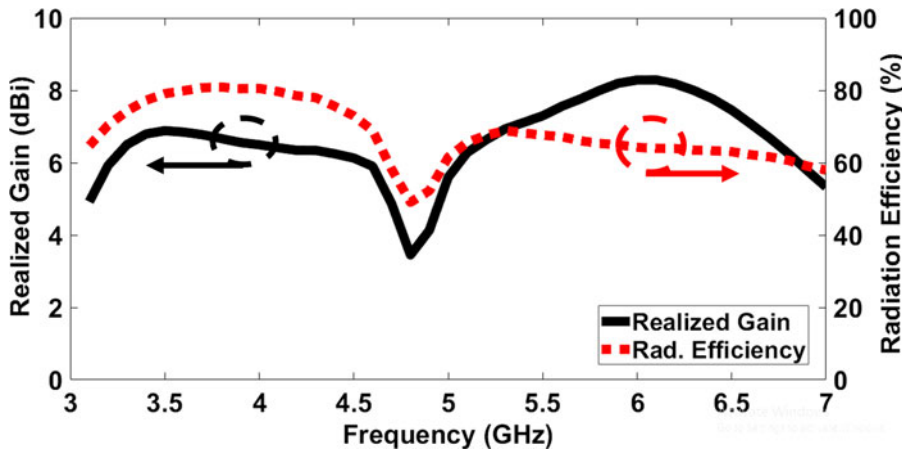


Fig. 4. The flat integrated antenna design simulated realized gain and radiation efficiency against the human wrist within the wideband spectrum.

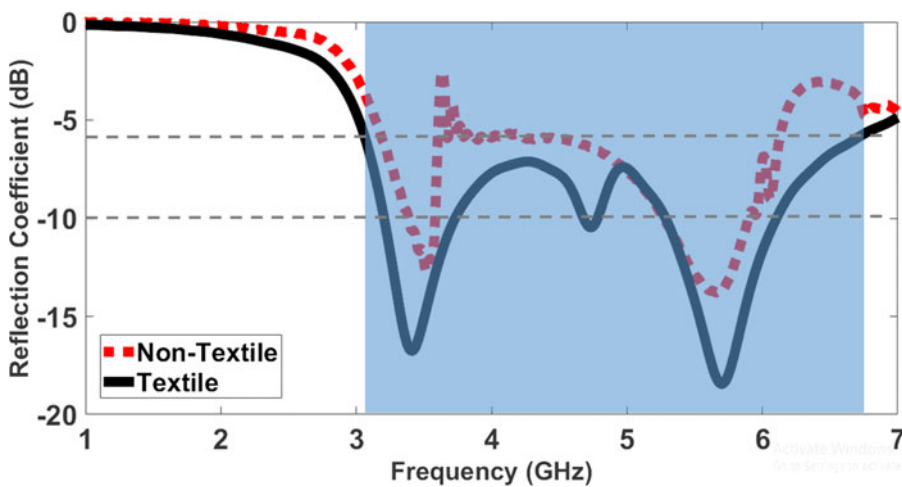


Fig. 5. Comparison with respect to the simulated integrated design reflection coefficients between the all-textile and polyimide-based designs.

design. This is considered the first advantage of utilizing textile materials over non-textile materials.

The second advantage is the high gain associated with the proposed all-textile-based design over the polyimide-based one. Putting emphasis on the two main resonant frequencies of 3.5 and 5.8 GHz, portrayed in Fig. 6 are the 3D gain radiation pattern of the all-polyimide design. As shown, the design exhibited gain values of 1.36 and 3.07 dBi at 3.5 and 5.8 GHz, respectively. Those values are lower than the proposed all-textile design, observed in Fig. 7, of 6.71 and 7.82 dBi at 3.5 and 5.8 GHz, respectively. This phenomenon was reported in [43], where it was described that textile antennas attain high gain due to the fact that the dielectric textiles dielectric constants are lower than polyimide ones. As such, the surface wave losses and spatial waves are minimized and improved, respectively.

From another point of view, SAR is calculated by defining the conductivity of the human tissue (σ), near-field electric field (E), and mass density of the human tissue (ρ) as stated in (1).

$$SAR = \frac{\sigma|E|^2}{\rho} \tag{1}$$

Thus, the all-textile flat integrated antenna design SAR levels, averaged over 1 g of tissue, at 3.5 and 5.8 GHz are highlighted in Fig. 8. A transmittal power level of 100 mW was input to the

antenna to guarantee fair and accurate benchmarking with the literature. The achieved peak SAR levels, averaged over 1 g of tissue, of 3.28×10^{-6} and 9.37×10^{-7} W/kg are considerably lesser than the threshold of 1.6 W/kg. Hence, in the flat circumstance, the all-textile integrated antenna design complies with the American standard and is safe to the human body. It is worth mentioning that the SAR value, averaged over 1 g of tissue, is lower at the higher band than at the lower band because the human body conductivity is higher at 5.8 GHz than at 3.5 GHz, as reported in [40] and [44]. Furthermore, due to the close separation with the human body, this in turn affected the antenna radiation efficiency, which decreased at the higher band than at the lower band, as was depicted in Fig. 4.

The bent all-textile integrated design performance against the human wrist

Due to the fact that the integrated design is all-textile, it is essential to evaluate its performance under bending scenarios. Hence, depicted in Fig. 9 is the all-textile bent integrated design over the SAM human hand phantom. The design was bent over angles of 20 and 40° along the X-axis. At such an arrangement, the all-textile integrated design was evaluated in terms of its performance parameters; for instance, the reflection coefficient, the 3D gain radiation pattern, and the SAR levels. Portrayed in the inset of Fig. 10 is the setup for measuring the all-textile bent integrated design fabricated prototype reflection coefficient over a subject's

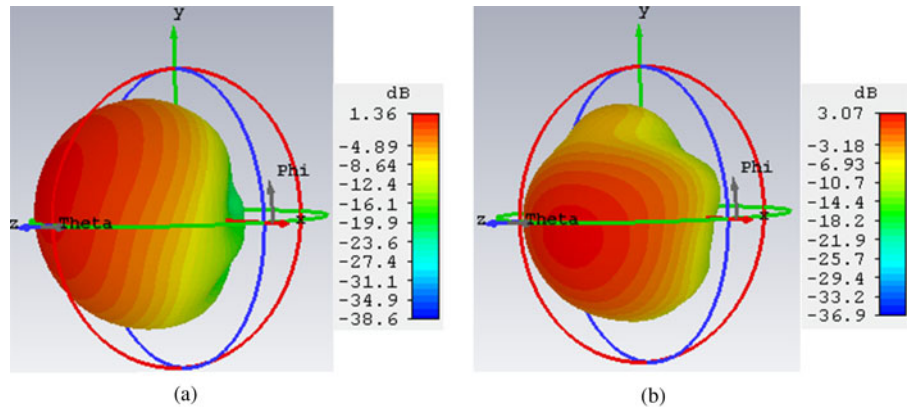


Fig. 6. The polyimide-based integrated design, placed on the SAM human hand phantom, 3D gain radiation pattern at: (a) 3.5 GHz; (b) 5.8 GHz.

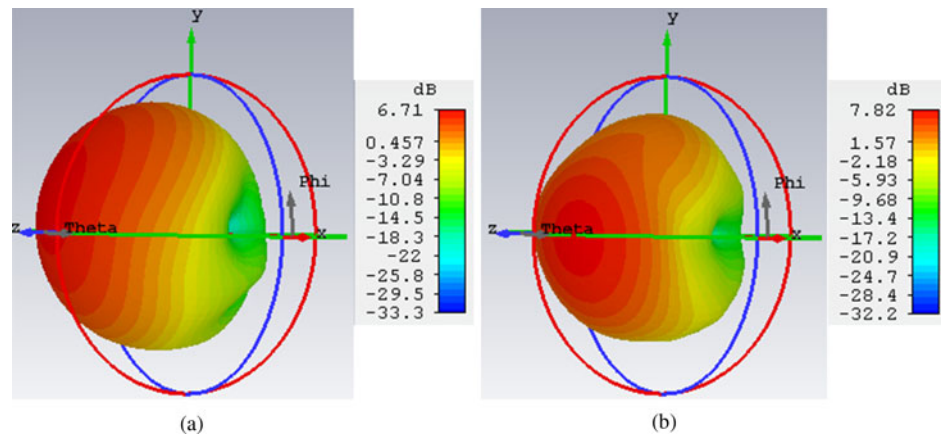


Fig. 7. The flat all-textile integrated design, placed on the SAM human hand phantom, 3D gain radiation pattern at: (a) 3.5 GHz; (b) 5.8 GHz.

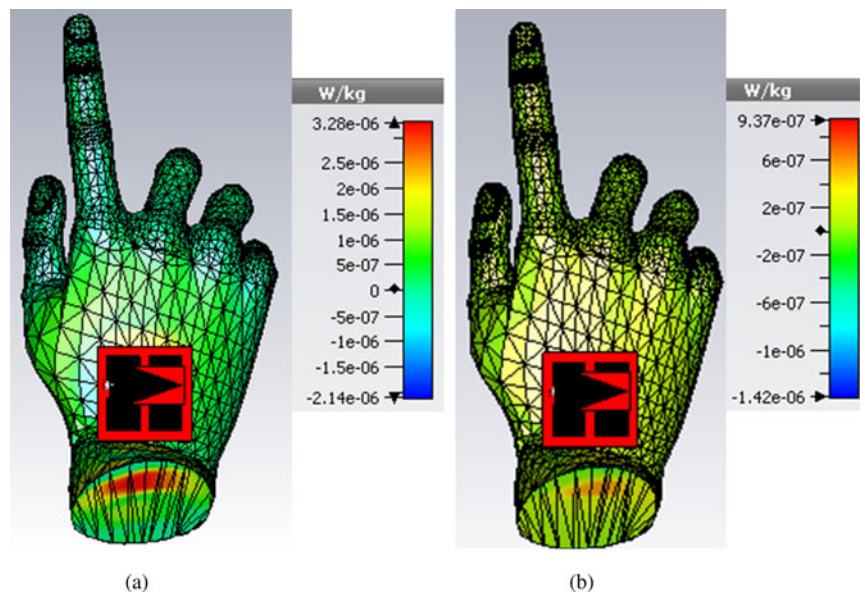


Fig. 8. The flat integrated antenna design SAR levels at: (a) 3.5 GHz; (b) 5.8 GHz.

wrist. As observed, the integrated design is mounted over a wrist-band to imitate the scenario targeted.

Compared in Fig. 10 are the simulated (solid black and dashed blue for 20 and 40° bents, respectively) and measured (dotted red) reflection coefficients. Whether bent at 20 or 40°, the integrated design achieved a wide-band resonance; however, the measured outcome was wider than was its simulated counterpart.

Furthermore, there are some frequency shifts that might be as a consequence of conducting fabrication manually, as well as the absence of the factors, that affect the measurement environment, in the simulation environment. The design displayed a simulated -6 dB impedance bandwidth ranging from 3.2 to 6.5 GHz (impedance bandwidth of 3.3 GHz). Whereas the attained measured -6 dB impedance bandwidth ranged from 2 to 6.5 GHz

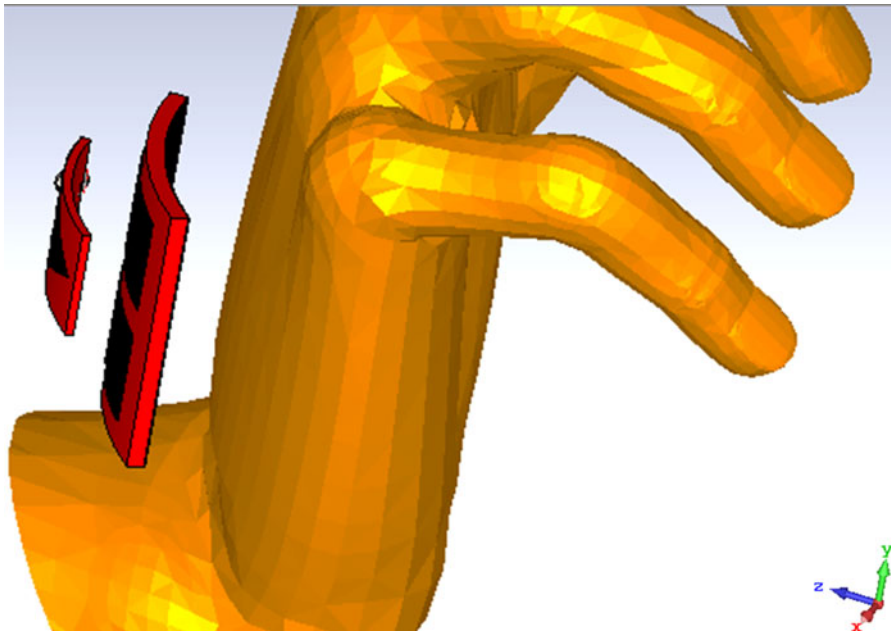


Fig. 9. The integrated design bent layout against the SAM human hand model.

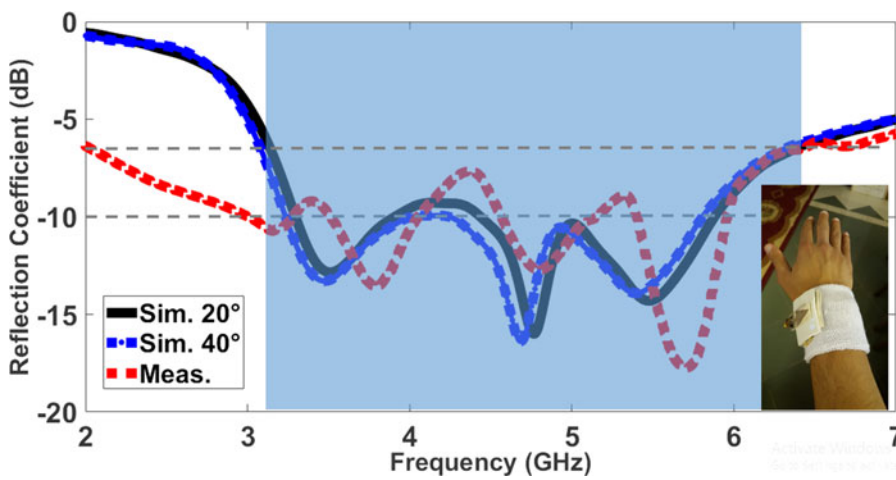


Fig. 10. Comparison between the simulated and measured bent integrated design reflection coefficients against the human wrist, with an inset of the setup for measuring the fabricated prototype reflection coefficient.

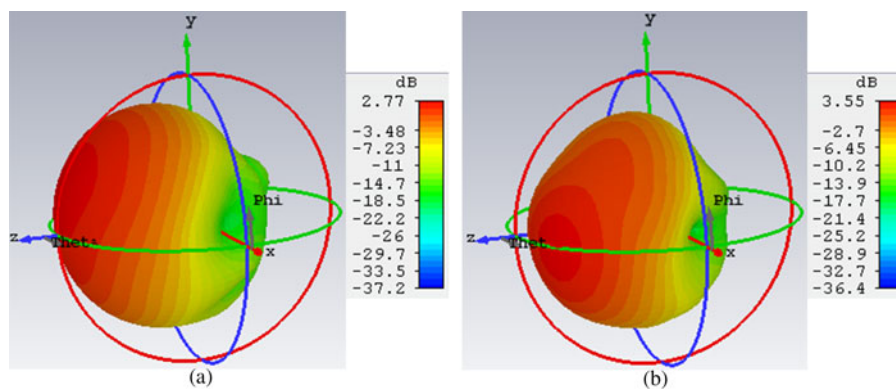


Fig. 11. The bent, at an angle of 20°, integrated antenna design 3D gain radiation pattern, against the SAM human hand phantom, at: (a) 3.5 GHz; (b) 5.8 GHz.

(impedance bandwidth of 4.5 GHz). As perceived, the bent case displayed a wider impedance bandwidth than the flat case, which could be due to the fact that the antenna was bent along the X-axis, which is the axis at which the antenna is excited.

Hence, the currents are highly disturbed and their paths are modified leading to different electrical lengths.

Portrayed in Fig. 11 are the all-textile bent, at an angle of 20°, integrated antenna design 3D gain radiation patterns at the two

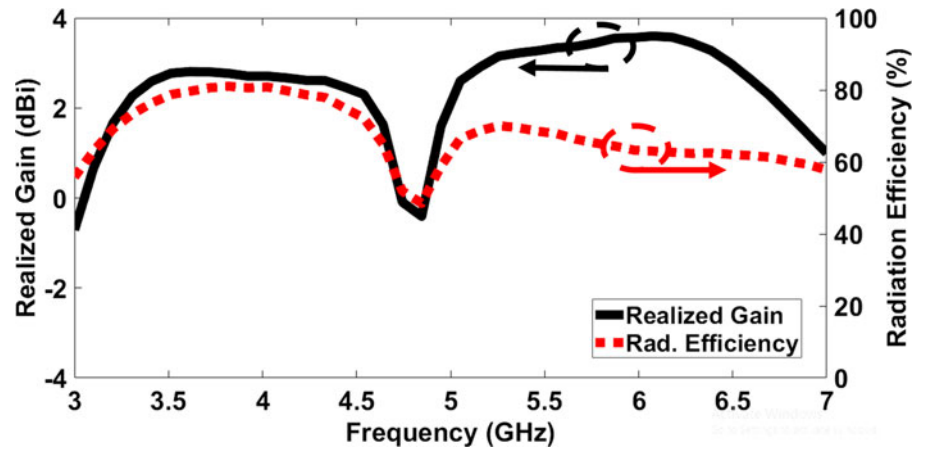


Fig. 12. The bent, at an angle of 20° , integrated design simulated realized gain and radiation efficiency against the human wrist.

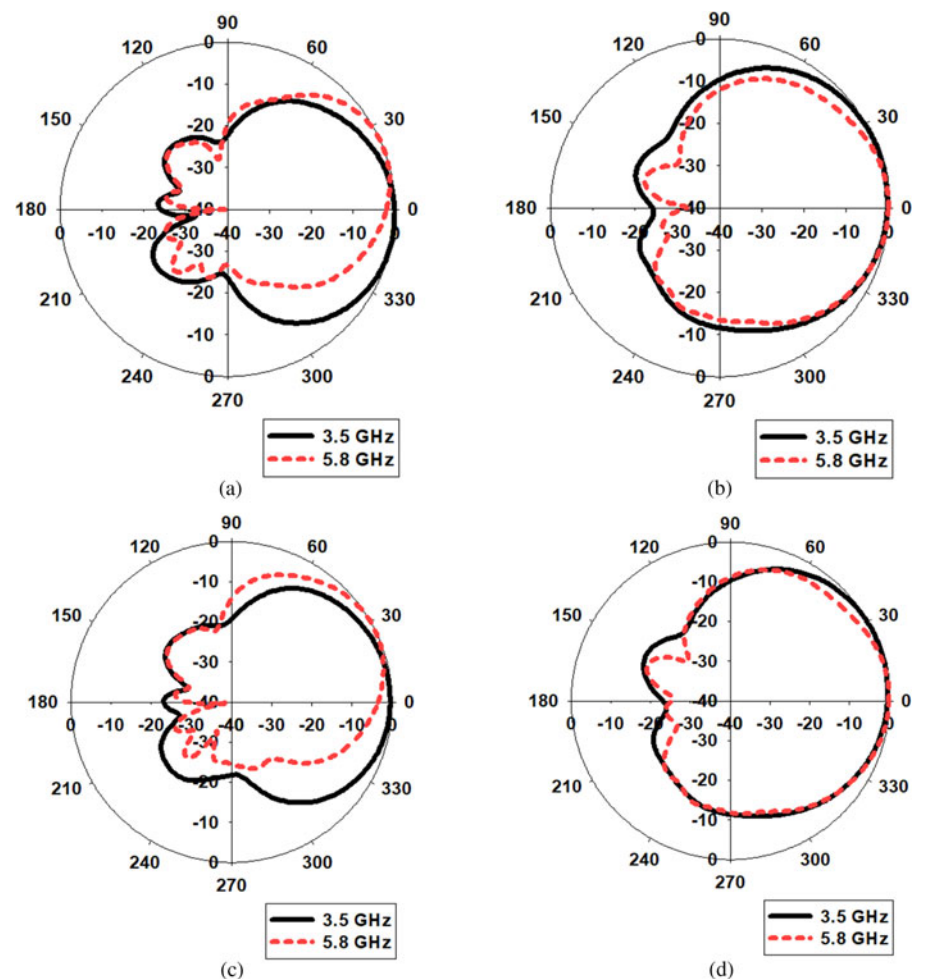


Fig. 13. Comparison between the integrated antenna design, placed over the SAM human hand phantom, normalized gain radiation pattern polar plots at 3.5 and 5.8 GHz when: (a) Flat in the E -plane, (b) Flat in the H -plane, (c) Bent, at an angle of 20° , in the E -plane, (d) Bent, at an angle of 20° , in the H -plane.

main resonant frequencies. The integrated design maintained its patch-like unidirectional pattern, courtesy of the reflecting AMC array structure. The antenna radiates in the boresight direction, which is along the positive Z -axis, as depicted in Fig. 11. This indicates that maximum power radiated is opposite to the human hand. At 3.5 and 5.8 GHz, the bent integrated antenna design attained peak realized gain of 2.77 and 3.55 dBi, as highlighted in Figs. 11(a) and 11(b), respectively. In addition, it

Table 1. The bent integrated antenna design peak SAR levels at 3.5 and 5.8 GHz

Antenna	Frequency (GHz)	Input power (mW)	SAR (W/kg) averaged over 1 g of tissue
Bent integrated design	3.5	100	3.34×10^{-6}
	5.8		9.43×10^{-7}

Table 2. Comparison between the characteristics and performances of the all-textile antenna and recent published antennas against the human body

Antenna	Resonant frequency (GHz)	Antenna electrical size (in terms of λ_0)/type/material/dielectric constant/dielectric thickness (mm)	Reflector physical size (mm ²)/type/material/dielectric constant/dielectric thickness (mm)	Realized gain (dBi)/radiation efficiency (%)	Input power (mW)/Max. SAR (W/kg) averaged over 1 g of tissue
Proposed	3.5/5.8	0.696 × 0.348 at 5.8 GHz/ Monopole/Felt (Textile)/1.2/1.5	45.3 × 45.3/AMC/Felt (Textile)/ 1.2/3	3.5 GHz: 6.71/79.1 5.8 GHz: 7.82/66.1	100/ 3.5 GHz: 3.28×10^{-6} 5.8 GHz: 9.37×10^{-7}
[2]	2.45	0.327 × 0.261 at 2.45 GHz/ Monopole/Felt (Textile)/1.2/2	81 × 81/EBG/Felt (Textile)/1.2/2	NA/NA	NA/0.554
[3]	2.45/5.8	0.619 × 0.754 at 5.8 GHz/CPW Monopole/Felt (Textile)/1.22/2	75 × 50/AMC/Felt (Textile)/1.22/2	2.45 GHz: NA/42 5.8 GHz: NA/51	NA/ 2.45 GHz: 0.86 5.8 GHz: 0.174
[4]	5.8	0.522 × 0.657 at 5.8 GHz/CPW Monopole/Pellon (Textile)/1.08/ 1.8	102 × 68/AMC/Pellon (Textile)/ 1.08/1.8	7.89/NA	1000/0.56
[5]	2.45	0.245 × 0.163 at 2.45 GHz/ Microstrip Monopole/Denim (Textile)/1.7/0.7	46 × 46/EBG/Denim (Textile)/1.7/ 0.7	NA/NA	100/0.0368
[6]	5.5	0.77 × 0.513 at 5.5 GHz/Probe-fed PIFA/Felt (Textile)/1.2/2	42 × 28/Metasurface/Felt (Textile)/1.2/2	NA/NA	500/0.3262
[8]	5.5	0.843 × 0.66 at 5.5 GHz/Probe-fed PIFA/Felt (Textile)/1.2/2	46 × 36/Ground Plane	5/64.2	500/0.9307
[9]	0.915/1.575	0.482 × 0.482 at 0.915 GHz/ Probe-fed Patch/Felt (Textile)/ 1.2/5	158 × 158/Ground Plane	0.915 GHz: −10.96/6.39 1.575 GHz: 8.26/ 72.61	1000/0.915 GHz: 0.175 1.575 GHz: 0.0252
[10]	2.45/5.5	0.653 × 0.653 at 2.45 GHz/ Probe-fed Patch/Textile/1.4/3	80 × 80/Ground Plane	2.45 GHz: 0.24/ 91.9 5.5 GHz: 4.51 (avg.)/86.3 (avg.)	NA/2.45 GHz: 0.2 5.5 GHz: 0.16 (avg.)
[11]	0.433/2.45	0.202 × 0.115 at 0.433 GHz/ Probe-fed PIFA/Felt (Textile)/1.3/ 6	140 × 80/Ground Plane	NA	NA
[21]	3.5/5.8	0.42 × 0.21 at 3.5 GHz/CPW Monopole/Rogers Ultralam 3850/ 2.9/0.1	86 × 86/AMC/RO3003/3/1.52	3.5 GHz: 9.373/ 83.5 5.8 GHz: 6.634/ 91.1	100/ 3.5 GHz: 0.0683 5.8 GHz: 0.333
[25]	UWB	1.547 × 1.295 at 5.8 GHz/ Probe-fed Microstrip Patch/ PDMS/2.7/3	80 × 67/Ground Plane	4.53 (avg.)/27 (avg.)	500/5 GHz: 0.147 7 GHz: 0.174 9 GHz: 0.09 (all avg. over 10 g of tissue)

achieved good radiation efficiencies of 78.74 and 64.43%, respectively.

Observing the left Y-axis scale of Fig. 12, the realized gain varied from 0.5 to 3.6 dBi; however, with a reduction to −0.4 dBi at 4.85 GHz. Moreover, perceiving the right Y-axis scale of Fig. 12, the radiation efficiency varied from 58 to 81%; though, with a reduction to 48.5% at 4.85 GHz. The reductions exhibited at 4.85 GHz are acceptable for bent textile wearable antennas. Moreover, the gain at 4.85 GHz is −0.1 dBi, which differs from the realized gain that takes into consideration the matching losses. Therefore, the integrated antenna design is robust against bending scenarios over the human wrist.

Furthermore, displayed in Fig. 13 is a comparison between the normalized gain radiation patterns in polar plots representation at both resonant frequencies and in the principal planes (X-Z and Y-Z planes). Figures 13(a) and 13(b) display such a comparison for the flat scenario in the X-Z plane and Y-Z plane, respectively. On the other hand, Figs 13(c) and 13(d) illustrate such a

comparison for the bent scenario, at an angle of 20°, in the X-Z plane and Y-Z plane, respectively. As observed, the antenna radiates in the $\theta = 0^\circ$ direction, which is normal to the user's hand. It is noticed that the main lobe direction is tilted to approximately 20° for the 5.8 GHz resonance in the X-Z plane, whether in the flat or bent scenarios. Yet, it is still acceptable since that direction is opposite to the human hand. Besides the good gain and radiation efficiency performances, the proposed all-textile integrated design displayed a high front-to-back ratio of 22 dB, as depicted in Figs 13(a) and 13(c), representing the X-Z plane. While in the Y-Z plane, it is 20 and 18 dB, in the flat (Fig. 13(b)) and bent (Fig. 13(d)) cases, respectively.

With a power level of 100 mW, the all-textile bent integrated antenna design SAR levels are tabulated in Table 1. At 3.5 and 5.8 GHz, it exhibited maximum SAR levels of 3.34×10^{-6} and 9.43×10^{-7} W/kg, averaged over 1 g of tissue, respectively. Similar to the flat case, it is worth noting that the SAR value, averaged over 1 g of tissue, is lower at the higher band than at the lower

band because the human body conductivity is higher at 5.8 GHz than at the lower resonant frequency, as reported in [40] and [44]. In addition, due to the close separation with the human body, this in turn affected the antenna radiation efficiency, which decreased at the higher band than at the lower band, as was demonstrated in Fig. 12. Hence, it is concluded that the antenna is robust against bending conditions and there are no health issues to be afraid of.

Finally, tabulated in Table 2 is a comparison between the all-textile proposed design and recent published antennas when evaluated within the vicinity of the human body. Comparison factors include the radiator electrical size and type, de-coupling structure size and type, substrate material, relative permittivity, thickness, realized gain, radiation efficiency, and SAR levels, averaged over 1 g of tissue. As tabulated, the proposed radiator electrical size is smaller than [3, 4] and [25], at 5.8 GHz. Furthermore, the suggested de-coupling structure is compact than all references besides [6]. Finally, the proposed integrated antenna design displayed the lowest SAR levels, averaged over 1 g of tissue, in comparison with the benchmarked references.

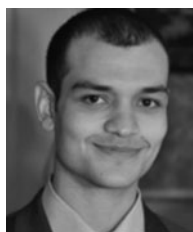
Conclusion

A wideband integrated wearable antenna consisting of a compact slotted triangular monopole antenna, of an overall form factor of $36 \text{ mm} \times 18 \text{ mm}$ (electrical size of $0.42 \lambda_0 \times 0.21 \lambda_0$ at 3.5 GHz), with a 3 mm-thick 2×2 textile AMC, of a physical size of $45.3 \text{ mm} \times 45.3 \text{ mm}$, was presented. Since the motivation was to design an integrated antenna for combination with a wristband for monitoring the human health conditions at the wrist, the design is all textile-based. Flat and bent simulations and measurements were conducted within the vicinity of the human wrist, precisely at a separation of 3 mm for the wristband. The integrated design achieved wideband resonance, where the emphasis was on the two main resonant frequencies of 3.5 and 5.8 GHz. The integrated design achieved acceptable high gain and radiation efficiency levels at both resonant frequencies. Furthermore, it is safe to the human wrist, according to the achieved SAR levels, averaged over 1 g of tissue, at both resonant frequencies. By displaying a wideband resonance, exhibiting high gain and radiation efficiency, as well as maintaining a high degree of flexibility, it is safe to say that the proposed all-textile integrated antenna design is greatly suggested for wearable WiMAX and medical applications.

References

- Hall PS and Hao Y (2012) *Antennas and Propagation for Body-Centric Wireless Communications*. Norwood, MA, USA: Artech House.
- Gao G-P, Hu B, Wang S-F and Yang C (2018) Wearable circular ring slot antenna with EBG structure for wireless body area network. *IEEE Antennas and Wireless Propagation Letters* 17, 1–4.
- Mersani A, Osman L and Ribero J-M (2018) Performance of dual-band AMC antenna for wireless local area network applications. *IET Microwaves, Antennas & Propagation* 12, 872–878.
- Alemaryeen A and Noghianian S (2018) On-body low-profile textile antenna with artificial magnetic conductor. *IET Microwaves, Antennas & Propagation* 12, 627–635.
- Ashyap AYI, Abidin ZZ, Dahlan SH, Majid HA, Mohd Shah S, Kamarudin MR and Alomainy A (2017) Compact and low-profile textile EBG-based antenna for wearable medical applications. *IEEE Antennas and Wireless Propagation Letters* 16, 2550–2553.
- Gao G-P, Yang C, Hu B, Zhang R-F and Wang S-F (2019) A wearable PIFA with an all-textile metasurface for 5 GHz WBAN applications. *IEEE Antennas and Wireless Propagation Letters* 18, 288–292.
- Hong Y, Tak J and Choi J (2016) An all-textile SIW cavity-backed circular ring-slot antenna for WBAN applications. *IEEE Antennas and Wireless Propagation Letters* 15, 1995–1999.
- Gao G-P, Yang C, Hu B, Zhang R-F and Wang S-F (2019) A wide-bandwidth wearable all-textile PIFA with dual resonance modes for 5 GHz WLAN applications. *IEEE Transactions on Antennas and Propagation* 67, 4206–4211.
- Lee H, Tak J and Choi J (2017) Wearable antenna integrated into military berets for indoor/outdoor positioning system. *IEEE Antennas and Wireless Propagation Letters* 16, 1919–1922.
- Xiaomu H, Yan S and Vandenbosch GAE (2017) Wearable button antenna for dual-band WLAN applications with combined on and off-body radiation patterns. *IEEE Transactions on Antennas and Propagation* 65, 1384–1387.
- Yan S, Volskiy V and Vandenbosch GAE (2017) Compact dual-band textile PIFA for 433-MHz / 2.4-GHz ISM bands. *IEEE Antennas and Wireless Propagation Letters* 16, 2436–2439.
- Chen SJ, Kaufmann T, Ranasinghe DC and Fumeaux C (2016) A modular textile antenna design using snap-on buttons for wearable applications. *IEEE Transactions on Antennas and Propagation* 64, 894–903.
- Poffelie LAY, Soh PJ, Yan S and Vandenbosch GAE (2016) A high-fidelity all-textile UWB antenna with low back radiation for off-body WBAN applications. *IEEE Transactions on Antennas and Propagation* 64, 757–760.
- Yan S and Vandenbosch GAE (2016) Radiation pattern-reconfigurable wearable antenna based on metamaterial structure. *IEEE Antennas and Wireless Propagation Letters* 15, 1715–1718.
- Hu B, Gao G-P, He L-L, Cong X-D and Zhao J-N (2016) Bending and on-arm effects on a wearable antenna for 2.45 GHz body area network. *IEEE Antennas and Wireless Propagation Letters* 15, 378–381.
- Paraskevopoulos A, Fonseca D dS, Seager RD, Whittow WG, Vardaxoglou JC and Alexandridis AA (2016) Higher-mode textile patch antenna with embroidered vias for on-body communication. *IET Microwaves, Antennas & Propagation* 10, 802–807.
- Yan S, Soh PJ and Vandenbosch GAE (2015) Wearable dual-band magneto-electric dipole antenna for WBAN/WLAN applications. *IEEE Transactions on Antennas and Propagation* 63, 4165–4169.
- Yan S, Soh PJ and Vandenbosch GAE (2015) Compact all-textile dual-band antenna loaded with metamaterial inspired structure. *IEEE Antennas and Wireless Propagation Letters* 14, 1486–1489.
- Liu F-X, Kaufmann T, Xu Z and Fumeaux C (2015) Wearable applications of quarter-wave patch and half-mode cavity antennas. *IEEE Antennas and Wireless Propagation Letters* 14, 1478–1481.
- Tak J and Choi J (2015) An all-textile Louis Vuitton logo antenna. *IEEE Antennas and Wireless Propagation Letters* 14, 1211–1214.
- El Atrash M, Abdalla MA and Elhennawy HM (2019) A wearable dual-band low profile high gain low SAR antenna AMC-backed for WBAN applications. *IEEE Transactions on Antennas and Propagation* 67, 6378–6388.
- El Atrash M, Abdalla MA and Elhennawy HM (2019) Gain enhancement of a compact thin flexible reflector-based asymmetric meander line antenna with low SAR. *IET Microwaves, Antennas & Propagation* 13, 827–832.
- Zahran SR, Abdalla MA and Gaafar A (2019) New thin wide-band bracelet-like antenna with low SAR for on-arm WBAN applications. *IET Microwaves, Antennas & Propagation* 13, 1219–1225.
- Jiang ZH, Cui Z, Yue T, Zhu Y and Werner DH (2017) Compact, highly efficient, and fully flexible circularly polarized antenna enabled by silver nanowires for wireless body-area networks. *IEEE Transactions on Biomedical Circuits and Systems* 11, 920–932.
- Simorangkir RBVB, Kiourti A and Esselle KP (2018) UWB Wearable antenna with full ground plane based on PDMS-embedded conductive fabric. *IEEE Antennas and Wireless Propagation Letters* 17, 493–496.
- Sabban A (2019) *Novel Wearable Antennas for Communication and Medical Systems*. Boca Raton, Florida, United States: CRC Press LLC.
- Sangeetha V, Sundarsingh EF, Kanagasabai M, Sarma AK, Sivasamy CRR and Pakkathillam JK (2015) Dual-band EBG integrated monopole antenna deploying fractal geometry for wearable applications. *IEEE Antennas and Wireless Propagation Letters* 14, 249–252.

28. **Sen Y, Soh PJ and Vandenbosch GAE** (2015) Dual-band textile MIMO antenna based on substrate-integrated waveguide (SIW) technology. *IEEE Transactions on Antennas and Propagation* **63**, 4640–4647.
29. **Lu WK, Chang H-J, Wang C-Y and Wang S-Y** (2020) Very-low-profile grounded coplanar waveguide-fed dual-band WLAN slot antenna for on-body antenna application. *IEEE Antennas and Wireless Propagation Letters* **19**, 213–217.
30. **Simorangkir RBVB, Yang Y, Matekovits L and Esselle KP** (2017) Dual-band dual-mode textile antenna on PDMS substrate for body-centric communications. *IEEE Antennas and Wireless Propagation Letters* **16**, 677–680.
31. **Simone G, Costa F, Fanciulli F and Monorchio A** (2016) Wearable inkjet-printed wideband antenna by using miniaturized AMC for sub-GHz applications. *IEEE Antennas and Wireless Propagation Letters* **15**, 1927–1930.
32. **Padmathilagam S, Kanagasabai M, Ramadoss S, Natarajan R, Alstath GN, Shanmuganathan S, Muthuramalingam S and Palaniswamy SK** (2020) Compact monopole antenna backed with fork slotted EBG for wearable applications. *IEEE Antennas and Wireless Propagation Letters* **19**, 228–232.
33. **Amor S, Iqbal A, Alazemi AJ, Waly MI, Ghayoula R and Kim S** (2020) Wideband wearable antenna for biomedical telemetry applications. *IEEE Access* **8**, 15687–15694.
34. **Alqadami ASM, Trong NN, Mohammed B, Stancombe AE, Tobias Heitzmann M and Abbosh A** (2020) Compact unidirectional conformal antenna based on flexible high permittivity custom-made substrate for wearable wideband electromagnetic head imaging system. *IEEE Transactions on Antennas and Propagation* **68**, 183–194.
35. **Zahran SR, Abdalla MA and Gaafar A** (2019) A flexible wide band single fed slot antenna with circular polarizing rotated elliptical ground and impulse response. *International Journal of Microwave and Wireless Technologies* **11**, 872–884.
36. **Sievenpiper DF, Zhang L, Broas RFJ, Alexopolous NG and Yablonoitch E** (1999) High-impedance electromagnetic surfaces with a forbidden frequency band. *IEEE Transactions on Microwave Theory and Techniques* **47**, 2059–2074.
37. **El Atrash M, Abdalla MA and Elhennawy HM** (2020) A compact flexible textile artificial magnetic conductor based wearable monopole antenna for low specific absorption rate wrist applications. *International Journal of Microwave and Wireless Technologies*, 1–7, in press.
38. **El Atrash M, Abdalgali OF, Mahmoud IS, Abdalla MA and Zahran SR** (2020) Wearable high gain low SAR antenna loaded with backed all-textile EBG for WBAN applications. *IET Microwaves, Antennas & Propagation* **14**, 791–799.
39. **El Atrash M, Abdalla MA and Elhennawy HM** (2020) A compact highly efficient Π -section CRLH antenna loaded with textile AMC for wireless body area network applications. *IEEE Transactions on Antennas and Propagation*, 1–10, in press.
40. **Mengjun W, Ze Y, Jianfei W, Jianhui B, Jianying L, Lulu C, Tao D, Hongxing Z and Erping L** (2018) Investigation of SAR reduction using flexible antenna with metamaterial structure in wireless body area network. *IEEE Transactions on Antennas and Propagation* **66**, 3076–3086.
41. **Specification Sheet – ShieldIt Super LessEMF Inc** (2013).
42. **Specification Sheet – Felt Sheet RS Components Inc** (2013).
43. **Rita S, Caroline L, Ricardo G and Pedro P** (2012) Textile materials for the design of wearable antennas: a survey. *Sensors* **12**, 15841–15857.
44. **Dielectric properties of body tissues**. Available at <http://niremf.ifac.cnr.it/tissprop/> (Accessed 02 August 2020).



Mohamed El Atrash received the B.Sc. degree (with honors) in electrical engineering from the Electrical Systems Engineering Department, October University for Modern Sciences and Arts (MSA), Cairo, Egypt, in 2011. He also received the M.Sc. degree (with distinction) in wireless mobile communications systems engineering from the University of Greenwich (UoG), UK, in 2014. Currently, he is pursuing his Ph.D. degree in electrical engineering at Ain Shams University, Cairo, Egypt. His research interests include flexible wearable antennas, high gain, thin, low profile antennas, and EBG/AMC design. Out of his research, he published articles in the *IEEE Transactions on Antennas & Propagation*, *IET Microwaves, Antennas & Propagation*, and the *International Journal of Microwave and Wireless Technologies*, as well as, a number of conference papers. He is a reviewer in the *IET Microwaves, Antennas & Propagation*, since 2019, where he has reviewed 15 journals.



Mahmoud A. Abdalla was born in 1973, received the B.Sc. and M.Sc. degrees in electrical engineering from Military Technical College, Cairo, Egypt in 1995 and 2000. He received the Ph.D. degree from the School of Electrical Engineering, University of Manchester, UK, in 2009. He is now a professor leading the electromagnetic waves group in Electronic Engineering Department, Military Technical College. Dr.

Mahmoud was the recipient of Egyptian encouragement state prize for engineering sciences in 2014. He published more than 200 peer-reviewed journal and conference papers. His research is focusing on miniaturized, multiband, and wideband microwave/millimeter antennas and components and also absorbing materials employing metamaterial/EBG, structures. He is a senior member of the IEEE/URSI and the European Microwave Association EuMA. He is a reviewer in many high ranked journals where he was awarded the top 1% Publons worldwide reviewer award for 2018 and 2019.



Hadia M. Elhennawy received the B.Sc. and M.Sc. degrees from Ain Shams University, Cairo, Egypt, in 1972 and 1976, respectively, and the Doctorate of Engineering (Dr.-Ing.) degree from the Technische Universität Braunschweig, Braunschweig, Germany, in 1982. Since 1992, she has been a Professor of communication engineering with the Electronics and Communications Engineering

Department, Ain Shams University. In 2004, she became a Vice-Dean for graduate study and research. In 2005, she became the Dean of the Faculty of Engineering, Ain Shams University. Her research interests include microwave devices and subsystems, as well as filters and antennas for modern radar and wireless communications applications.